IJCRT.ORG ISSN : 2320-2882

INTERNATIONAL JOURNAL OF CREATIVE RESEARCH THOUGHTS (IJCRT)

An International Open Access, Peer-reviewed, Refereed Journal

Numerical Modelling of High-Speed Rail Embankment

[1]Maran T. G. Salib, [2]Tamer M. Sorour
Department of Structural Engineering, Ain Shams University, Cairo, Egypt

Abstract: Advanced numerical simulation is required to accurately capture the dynamic impact loads that high-speed rail systems impose on subsurface soils. High-speed rail systems impose dynamic loads that require advanced modeling to accurately assess their impact. This study develops a three-dimensional finite element model in PLAXIS 3D to simulate the dynamic response of a ballasted railway track subjected to high-speed train loading. Two constitutive soil models are evaluated: a simplified Linear Elastic (LE) model and a more advanced Hardening Soil model with Small-Strain stiffness (HSS). While both models provide reasonable predictions of dynamic response under the track, the HSS model demonstrates improved performance in capturing vibration attenuation and settlement behavior in the surrounding soil. The HSS model is attributed to its ability to account for non-linear stress–strain behavior and strain-dependent stiffness degradation, which the LE model does not capture. The findings emphasize the limitations of using purely elastic models for dynamic railway analysis and highlight the benefits of adopting more realistic constitutive models. The HSS model is shown to be more suitable for simulating subsoil behavior under high-speed train loading, particularly in areas where accurate prediction of ground deformation and vibration is critical.

Keywords: High-Speed train, Linear elastic, Hardening soil with small strain, 3D model, settlement.

I.INTRODUCTION

According to the International Union of Railways (UIC), high-speed rail is typically defined as rail systems operating at speeds exceeding 250 km/h on new lines and 200 km/h on existing upgraded lines [1]. High-speed trains (HSTs) generate complex dynamic loads on railway infrastructure, particularly affecting the track–subgrade–soil interaction system. These loads can induce significant long-term deformations, vibration propagation, and degradation of subsoil properties.

The earliest modeling approaches simplified train loads as equivalent static forces, applying the vertical axle loads at fixed positions on the track. This approach was sufficient for preliminary design and low-speed analysis but failed to capture essential dynamic effects such as wave propagation, resonance, and critical velocity effects. To account for the increased impact of moving loads at higher speeds, a dynamic amplification factor (DAF) is often applied to the static load. This factor served as a simplified means to estimate the additional forces induced by dynamic effects such as [2] and [3]

With the increasing demand for high-speed railway operations, understanding the dynamic behaviour of track structures under moving loads has become essential in railway engineering. Early theoretical investigations were first initiated by [4], who studied the response of an elastic half-space subjected to impulsive loads. Many later works have continued to seek solutions for the problem of the elastic response to harmonic loads. This work led to the identification of different wave types generated by such loads, including compression waves (P-waves), which move particles in the direction of propagation; shear waves (S-waves), which move particles perpendicular

to the direction of travel; and Rayleigh waves (R-waves), which occur at the surface and decrease in amplitude with depth.

One of the most widely used analytical approaches in track modelling is the Beam on Elastic Foundation (BOEF) model, originally developed by Winkler. This model simulates the rail as an infinitely long Euler-Bernoulli beam supported by discrete vertical springs and dampers that represent the track foundation. The BOEF model can be applied in two ways: one approach models only the rail as a beam, while the underlying layers (sleepers, ballast, subgrade) are simulated as the foundation; the other approach includes more of the superstructure (rail, sleepers, ballast) as part of the beam, with the subgrade modelled as the foundation.

The linearity of the model allows for the principle of superposition, meaning the total track response under multiple axle loads can be determined by adding the responses from each individual load. This makes it suitable for analyzing train-induced effects in a simplified manner. It is widely used to estimate rail deflection and serves as a reference for validating more advanced numerical models. However, the model has technical limitations. It does not account for shear stress transfer between track layers and is based on several idealized assumptions, which may limit its accuracy when applied to complex track conditions.

The limitations of analytical models prompted a shift toward dynamic modeling techniques. The Finite Element Method (FEM) is a fundamental tool in geotechnical engineering offering detailed predictions of stresses, displacements, and dynamic responses in complex soil–structure systems without presuming failure modes. Its capability to incorporate realistic track geometries and advanced soil constitutive models makes it particularly effective for simulating railway track behavior under train-induced dynamic loading [5], [6].

However, accurate modelling requires careful treatment of model boundaries to prevent artificial wave reflections caused by dynamic loads. Several solutions have been proposed, such as moving boundaries far from the loading area or using non-reflecting viscous boundaries [7], [8]. More advanced methods, including infinite elements and the Scaled Boundary Finite Element Method [9], have further improved wave absorption.

FEM can be implemented in two or three dimensions: 2D plane strain models are simpler and computationally efficient but require the assumption of uniform track geometry along the longitudinal direction, limiting their ability to capture discrete sleeper supports and accurate longitudinal load distribution [10].

Conversely, 3D FEM models overcome these limitations by fully representing the track structure, sleeper spacing, and load distribution in all directions, providing results that align well with field measurements [11]. Despite their accuracy, 3D models demand significantly higher computational resources, making the choice between 2D and 3D modelling dependent on the required precision and available resources.

This study contributes to this body of work by developing a three-dimensional finite element numerical model that incorporates the essential dynamic features of high-speed train loading and the effect of different constitutive laws on the behavior of dynamic loading compared to equivalent static loading.

II. NUMERICAL MODELLING

2.1 Case study

The case study focuses on the Thalys high-speed train ballasted track. It is a double track located near Ath, 55 km south of Brussels. The superstructure of the track consists of continuously welded UIC60 rails. The rails are fixed to precast prestressed monoblock concrete sleepers using fasteners with a 0.01m rail pad placed between the rail and the sleepers. All the above elements are rested on a 1.0 m height embankment. Due to the missing data of embankment geometry and properties, they were taken according to another site near the case study located in Mons in the south of Leuze-en-Hainaut in Belgium, mentioned by [12] and [13], as shown in **Figure 1**.

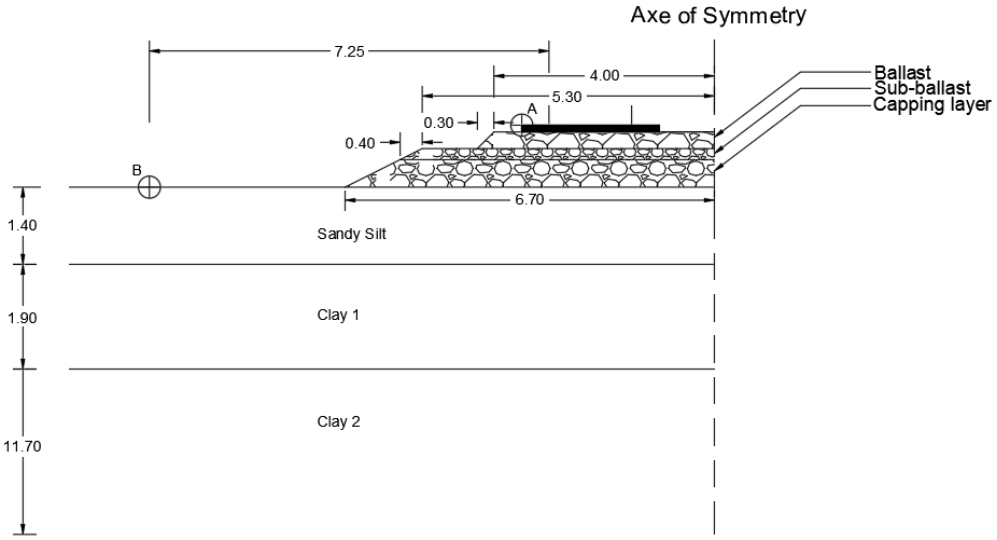

Figure 1. Configuration of the problem studied. (Accelerometer A was used for measurements of track acceleration versus time while accelerometer B was used for measurements of ground acceleration versus time.)

The dynamic properties of the soil were determined using the Spectral Analysis of Surface Waves (SASW) method. This technique is based on the dispersive behavior of Rayleigh waves as they propagate through layered soil medium. In the test, A transient excitation was produced by dropping a 110 kg mass from a height of 0.9 m onto a square steel foundation (0.7 m per side) with a mass of 600 kg.

Vertical ground surface responses are then recorded at multiple depths from the impact point using geophones or accelerometers placed on the soil surface. Based on the measured responses, the theoretical dispersion curve of the soil is derived using the Haskell-Thomson method. An inverse problem is then formulated, where the shear wave velocity profile with depth is iteratively adjusted in a numerical model to minimize the discrepancy between the measured and computed dispersion curves.

It is important to note that a single experimental dispersion curve may correspond to multiple possible shear wave velocity profiles. Additionally, the test data can be used to derive the soil's attenuation curve. By solving a similar inverse problem, the shear damping ratio profile with depth can be estimated. According to shear wave velocity values recorded by SASW test for the investigated depths (up to 15.0 m below the ground level), the native soil consists of Sandy Silt layer followed by two different layers of Clay. [14].

In addition to the variation of soil stiffness with depth, it was necessary to estimate the hysteretic material damping. Data obtained from cone penetration tests and Spectral Analysis of Surface Waves (SASW) indicated that the subsurface profile was not homogenous, suggesting that the damping ratio (ξ) may vary with depth. Despite this, [15] employed the classical Barkan expression, which assumes a homogeneous elastic half-space. Within this simplified framework, an inverse analysis was conducted, leading to the adoption of a constant damping ratio of $\xi = 3\%$. All the properties of superstructure from field investigation are summarized in Table 1

Table 1-Properties of Track superstructure from field measurements provided by [15], [10], [12] & [13].

Element	Material Property	Value	Unit
Rail	Elastic Modulus	210,000.	MPa
	Poisson's ratio	0.30	-
	Moment of Inertia, I (m^4)	3.055×10^{-5}	m^4
	Unit Weight	78.00	kN/m^3
Sleepers	Elastic Modulus	30,000	MPa
	Unit Weight	20.54	kN/m^3
	Poisson's ratio	0.20	-
	Length	2.50	m
	Width	0.285	m
	Height	0.205	m
Ballast	Elastic Modulus	100.00	MPa
	Poisson's ratio	0.35	-
	Unit Weight	18.00	kN/m^3
	Thickness	0.30	m
	Damping ratio	1.00	%
	Friction angle*	40	degrees
Sub-ballast	Elastic Modulus	300.00	MPa
	Poisson's ratio	0.35	-
	Unit Weight	22.00	kN/m^3
	Thickness	0.20	m
	Damping ratio	1.00	%
	Friction angle*	45	degrees
Capping Layer	Elastic Modulus	127	MPa
	Poisson's ratio	0.35	-
	Unit Weight	21.00	kN/m^3
	Thickness	0.50	m
	Damping ratio	1.00	%
	Friction angle*	42	degrees

*Assumed values

Thalys train is a high-speed train with a maximum speed of 314 km/h. It consists of 2 locomotives and 8 carriages with total length of 200.18 m. The train configuration consists of a locomotive supported by two bogies with four axles in total. The carriage directly adjacent to the locomotive shares one bogie with it, while the remaining six carriages are connected in pairs, each pair sharing both bogies with neighboring carriages. In total, the train has 13 bogies and 26 axles. The characteristics of the Thalys HST are summarized in **Table 2.**

Table 2-Geometry and characteristics of Thalys Train provided by [16]

Carriage Name	Carriage Number	Axle per Carriage	Spacing			M_t (kg)
			L_t (m)	L_b (m)	L_a (m)	
Locomotive	2	4	22.15	14.00	3.00	17000
Side Carriage	2	3	21.84	18.70	3.00	14500
Central Carriage	6	2	18.70	18.70	3.00	17000

2.2 Geometric configuration of finite element modelling

A three-dimensional finite element model was developed and analyzed using the commercially available software PLAXIS-3D V2021. A sensitivity analysis was carried out to identify the minimum model boundary dimensions and finite element mesh size needed to reduce boundary and mesh-related effects on the numerical results, while maintaining a reasonable computational time. The model dimensions are 100 m (x-direction), 60 m (y-direction) and 50 m (z-direction) as shown in
Figure 2.

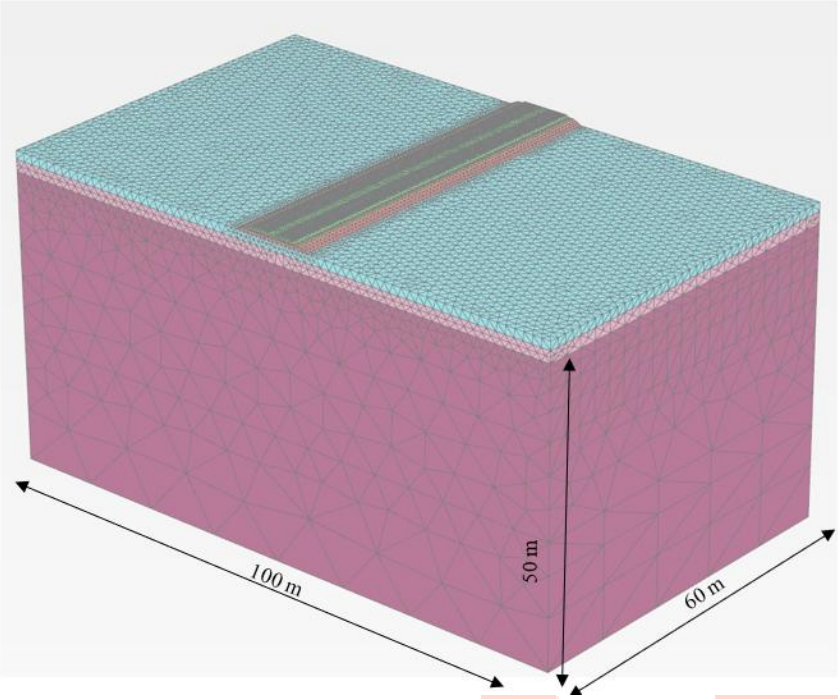

Figure 2. Finite element numerical model and generated mesh.

These dimensions were determined following a sensitivity analysis that evaluated the influence of the normalized model width on ground surface settlement beneath the rail, at point B and near the model boundary. The results indicated that settlement directly beneath the rail remained essentially unaffected by changes in model width, whereas settlements at point B and the boundary exhibited noticeable variation with increasing width as shown in
Figure 3.

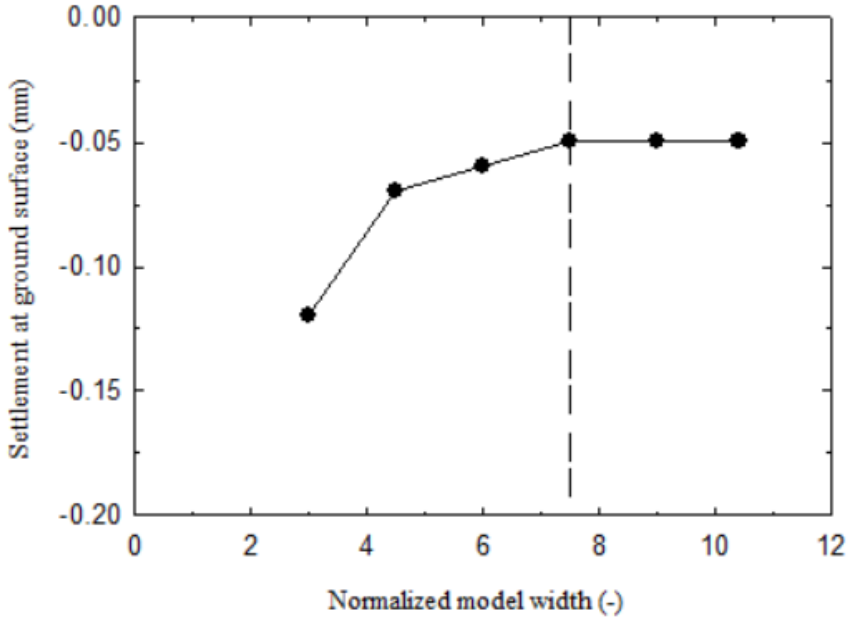

(a) Variation of normalized width versus ground settlement

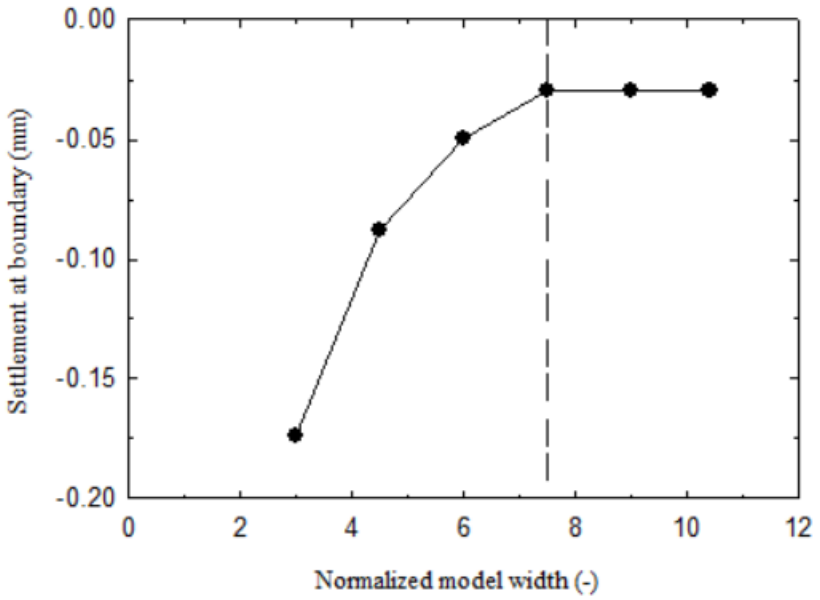

(b) Variation of normalized width versus ground settlement

Figure 3. (a) Variation of normalized width versus ground settlement. (b) Variation of normalized width versus boundary settlement. Normalized model width = Model width divided by embankment width.

Moreover, the optimum mesh size required to generate accurate results within a manageable time is very fine mesh with a variable coarseness factor along the model. The coarseness factor is 0.25 for the track elements and embankment layers, 0.50 for the sandy silt layer and 1.00 to 4.00 for the clay layers. Viscous dampers are applied at the vertical boundaries of the model to absorb incoming S- and P-waves, effectively simulating infinite boundary conditions. [17].

2.3 Material models

The rail is modeled as a 1D I-beam (UIC section) along the full length of the track. Other parts of the track, including the embankment layers, are modeled using 3D solid elements. A total of 100 sleepers are placed along the rail, spaced 0.6 meters apart. The rail and sleepers are defined as linear elastic materials while the embankment layers are modelled using Mohr-Coulumb (MC) constitutive law.

The soil layers were modeled twice, first using a Linear Elastic (LE) model and then using the Hardening Soil model with small-strain stiffness (HSS), to investigate the influence of soil constitutive behavior on the settlement.

The Linear Elastic (LE) model represents soil as a perfectly elastic medium in which stress and strain are related by constant stiffness parameters, such as Young's modulus and Poisson's ratio. It assumes no permanent deformation and does not account for stiffness variation with stress level or strain amplitude, making it most suitable for preliminary analyses or materials with purely elastic behavior. In contrast, the Hardening Soil Small-Strain (HSS) model is an advanced constitutive model that incorporates stress-dependent stiffness, plastic deformation, and a strain-dependent stiffness degradation at very small strains. It captures the observed increase in soil stiffness at low strain levels and its gradual reduction as strain increases, enabling more realistic simulation of soil behavior under cyclic or transient loads. Conceptually, while the LE model provides a simplified, idealized response, the HSS model reflects a more physically accurate representation of soil nonlinearity, stiffness hardening, and small-strain effects.

Table 3- Soil parameters used in the linear elastic model.

Parameter	Sandy Silt	Clay 1	Clay 2
Thickness (m)	1.40	1.90	46.70
γ_{bulk} (kN/m^3)[1]	18.50	18.50	18.50
γ_{sat} (kN/m^3)[2]	18.50	18.50	18.50
E (kPa)[3]	48000	85000	250000
υ (-)	0.30	0.30	0.30
ξ[4]	3.00	3.00	3.00

[1] Bulk unit weight of soil; [2] Saturated unit weight of soil; [3] Dynamic soil modulus; [4] Damping ratio.

Table 4- Soil parameters used in the small strain hardening soil model.

Parameter	Sandy Silt	Clay 1	Clay 2
Thickness	1.40	1.90	46.70
γ_{bulk} (kN/m^3)[1]	18.50	18.50	18.50
γ_{sat} (kN/m^3)[2]	18.50	18.50	18.50
E_{50}^{ref} (kPa)[3]	2912.50	15812.50	51875.00
E_{oed}^{ref} (kPa)[4]	2330.00	12650.00	41500.00
E_{ur}^{ref} (kPa)[5]	8737.50	47437.50	155625.00
m (-)[6]	0.50	1.00	1.00
υ_{ur} (-)[7]	0.20	0.20	0.20
s_u (kPa)[8]	NA[16]	40.00	170.00
c' (kPa)[9]	2.00	4.00	17.00
$\emptyset$' (degree)[10]	28.00	27.00	28.00
Ψ (degree)[11]	0.00	0.00	0.00
OCR (-)[12]	NA[16]	5.00	9.00
G_0^{ref} (kPa)[13]	41500	39480	82585
$\gamma_{0.7}$ (-)[14]	0.0003	0.0004	0.0003
ξ[15]	3.00	3.00	3.00

[1] Bulk unit weight of soil; [2] Saturated unit weight of soil; [3] 50% secant soil modulus in triaxial test defined at a reference minor principal effective stress of 100 kPa; [4] Tangent soil modulus from oedometer test for one dimensional compression at a reference minor principal effective stress of 100 kPa; [5] Unloading-reloading soil modulus; [6] Power relating stiffness to stress value; [7] Unloading-reloading Poisson's ratio; [8] Undrained shear strength; [9] Effective cohesion strength; [10] Internal friction angle; [11] Dilatancy angle; [12]Over consolidation ratio; [13] Initial Shear modulus; [14]Shear strain level $\gamma_{0.7}$ at which the secant shear modulus G_s is reduced to about 70% of G_0.; [15] Damping ratio [16] Not applicable.

2.4 Rayleigh damping in finite element modelling

In the finite element (FE) model, material damping is represented through mass- and stiffness-proportional coefficients, a formulation commonly known as Rayleigh damping. This approach is widely adopted in nonlinear dynamic analyses because it provides a practical means of approximating energy dissipation over a range of frequencies. The Rayleigh damping relationship is expressed as:

$$C = \alpha M + \beta K \quad (1)$$

where C is the damping matrix, M is the mass matrix, K is the stiffness matrix, α is the mass-proportional damping coefficient, and β is the stiffness-proportional damping coefficient. These coefficients are frequency-dependent and are typically determined using the expressions proposed by [18]:

$$\alpha = \frac{2\omega i \omega j(\xi i \omega j - \xi j \omega i)}{\omega j^2 - \omega i^2} \quad (2)$$

$$\beta = \frac{2(\xi j \omega j - \xi i \omega i)}{\omega j^2 - \omega i^2} \quad (3)$$

where ω_i and ω_j are the angular frequencies of the first and second modes, respectively, and ξ_i and ξ_j are the corresponding hysteretic damping ratios.

Selecting appropriate target frequencies for calibration is crucial to accurately representing damping behavior. [19] recommend that the first target frequency f_1 corresponds to the first natural frequency of the soil deposit, while the second target frequency should be the nearest odd multiple greater than the ratio f_p/f_1, where f_p is the predominant frequency of the input motion obtained from its Fourier spectrum or field measurement. The first natural frequency of the soil f_1 can be estimated from:

$$f1 = \frac{Vs}{4H} \quad (4)$$

where Vs is the average shear wave velocity and H is the total thickness of the soil deposit. This calibration ensures that the Rayleigh damping parameters effectively capture the relevant frequency range of the dynamic response.

2.5 Load simulation

One of the primary challenges lies in accurately modeling the moving load. This can be approached using two distinct methodologies. The frequency domain approach examines the wheel response to a “moving irregularity” by analyzing system behavior in the spectral domain. Alternatively, the time domain approach utilizes a numerical time-stepping scheme to simulate the dynamic interaction between the train and the track over time.

In the present study, a time-domain numerical approach was employed, following the methodologies developed by [20], [21]. All simulations were conducted using direct time integration schemes with implicit solvers, ensuring stability and accuracy in the dynamic analysis. The train moving load was modeled according to [22]. Specifically, the rail was rigidly connected to the sleepers, and a single time-varying wheel load was assigned to each finite element (FE) node situated above the rail. The moving load was simulated as a triangular pulse, distributed across three nodes: the central node and its two adjacent nodes. As the load transitioned from node N to node N+1, the applied force at node N+1 increased progressively, reaching its maximum when the load was directly above that node. Subsequently, as the load continued towards node N+2, the force at node N+1 decreased gradually to zero. This approach allowed the triangular load pulse to propagate from node to node over a specific time interval, defined by the spacing between nodes divided by the speed of the moving load. For example, at a train speed of 314 km/h (87.22 m/s), the wheel point load travels the 0.60 m distance between two consecutive loading nodes in approximately 0.007 seconds. This rapid progression of loads along the track creates a continuous sequence of moving wheel loads that interact dynamically with the track–ground system.

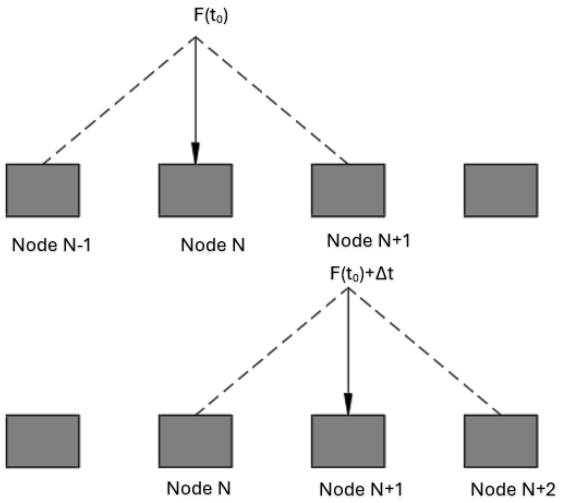

Figure 4 Modelling of the moving load.

An equivalent static model was also developed using the American Railway Engineering and Maintenance-of-Way Association (AREMA) methodology [3]. The static model was employed to investigate the influence depth of the applied loading and its effect on the stress distribution within the soil profile compared with the dynamic approach.

For the static loading, the design load P applied to the model was calculated using the relationship

$$P = IF \times \frac{2qr}{L} \times DF \quad (5)$$

where the impact factor IF is given by:

$$IF = 1 + 5.21 \times \frac{V}{D} \quad (6)$$

and the distribution factor DF by:

$$DF = \frac{(0.061 \times S) + 13.37}{100} \quad (7)$$

In these expressions, q_r denotes the rail seat load, L the sleeper length, V the train speed in km/hr, D the wheel diameter in mm, and S the sleeper spacing in mm.

III. RESULTS AND DISCUSSIONS

3.6 Effect of soil model on settlement

For further detailed comparison between the two material models, four observation points were selected to evaluate the variation of settlement over dynamic loading time. Point B is located 7.25 m from the rail, with point C positioned 1.0 m directly beneath it. The remaining two points are located between the rails, where the maximum load is applied: Point E lies at the ground surface, while point D is positioned 1.0 m below Point E as shown in **Figure 5**.

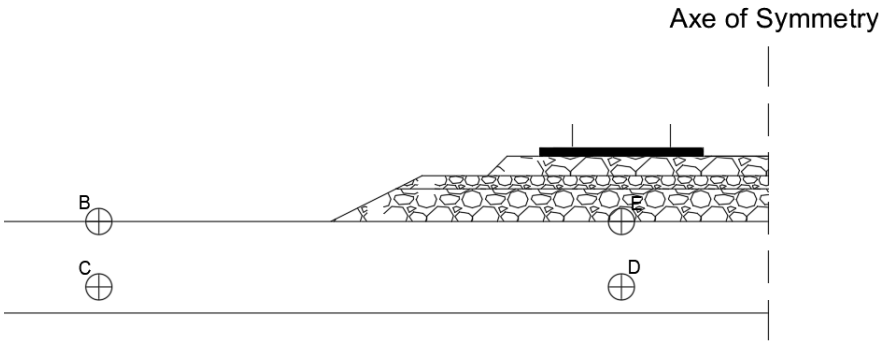

Figure 5. Location of chosen points to compare the settlement variation versus time using linear elastic and small strain hardening soil models.

The variation of ground settlement with dynamic time for the four selected observation points is illustrated in **Figure 6**. In general, the settlements directly beneath the applied load, such as at points D and E, are greater in the HSS model compared to the LE model. This is primarily because the HSS model accounts for strain-dependent stiffness and shear modulus (G) degradation, which leads to a reduction in stiffness at higher strain levels beneath the load. By contrast, the LE model assumes constant stiffness regardless of strain level, thereby underestimating deformation in zones of high strain.

For locations farther from the load, such as Points B and C, the trend is reversed: the LE model predicts slightly higher settlements than the HSS model. This occurs because strain levels are lower in these regions, and the HSS model retains a higher small-strain stiffness (G_0) that resists deformation more effectively. Furthermore, the difference in settlement between the two models at Point E is greater than at point D, as point E is at the ground surface and therefore experiences higher strain amplitudes due to direct loading, while point D, located 1.0 m below, experiences attenuated strain and reduced modulus degradation.

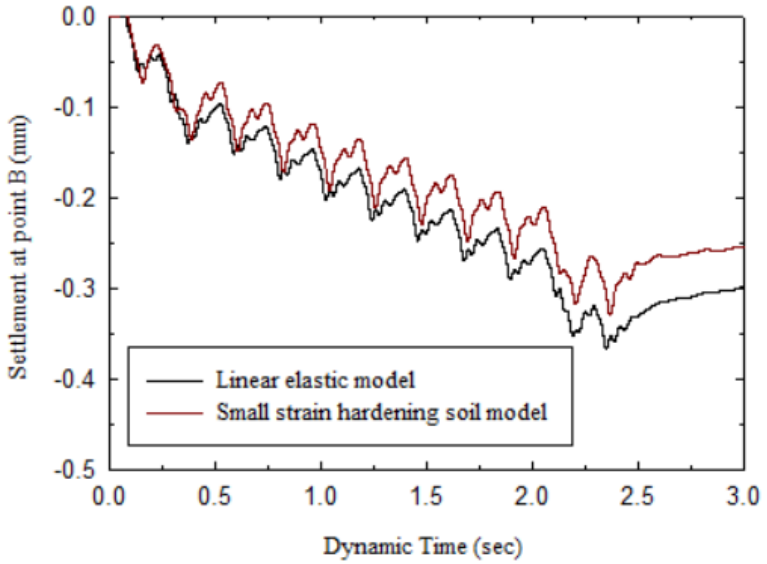

(a) Variation of ground settlement with dynamic time at point B.

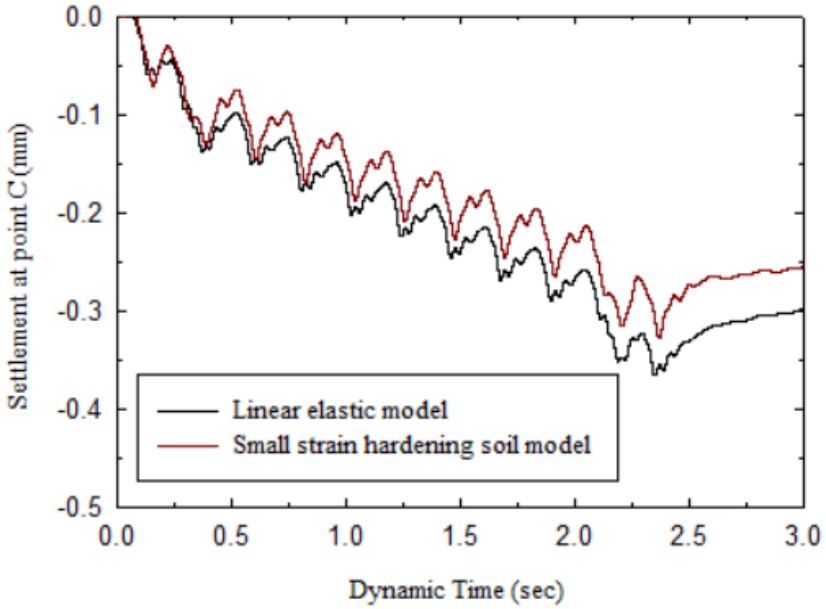

(b) Variation of ground settlement with dynamic time at point C.

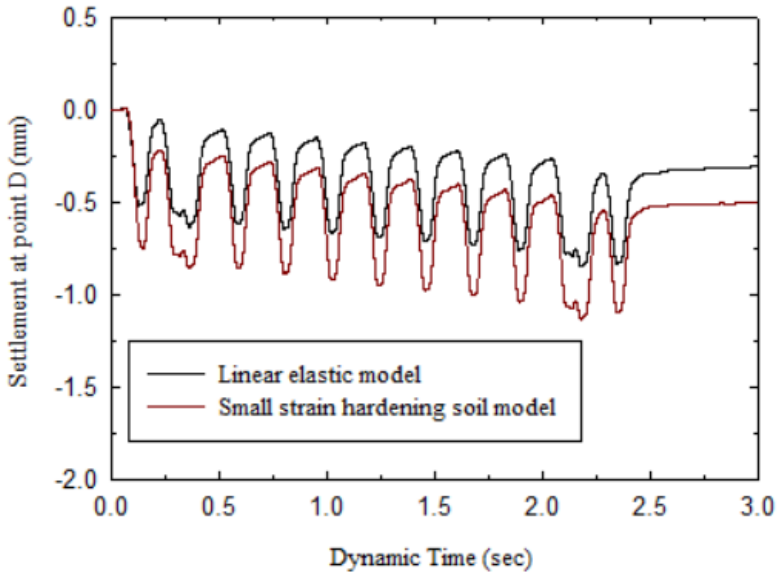

(c) Variation of ground settlement with dynamic time at point D.

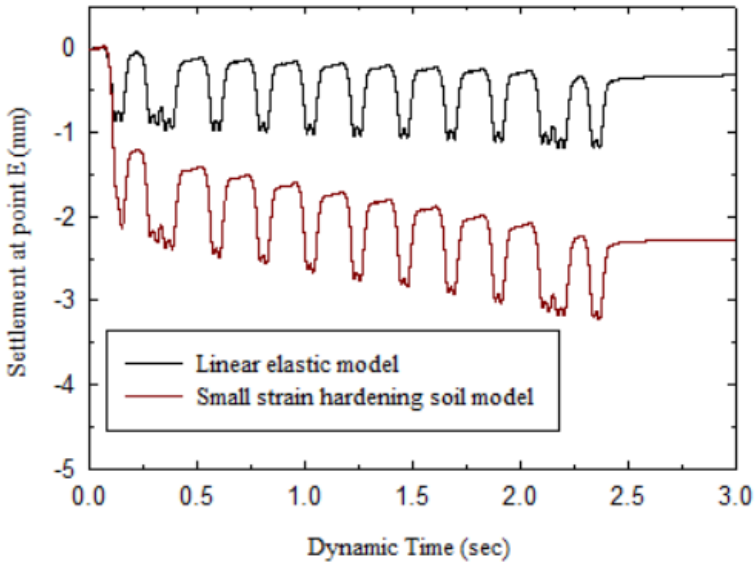

(d) Variation of ground settlement with dynamic time at point E.

Figure 6. Comparison of variation of ground settlement versus dynamic time between linear elastic model and small strain hardening soil model. (a) Comparison ground settlement versus dynamic time at point B. (b) Comparison ground settlement versus dynamic time at point C. (c) Comparison ground settlement versus dynamic time at point D. (d) Comparison ground settlement versus dynamic time at point E.

3.7 Effect of load configuration on influence depth

Analysis of the vertical stress distribution indicates that the effective depth of influence from the train loading varies significantly depending on the loading simulation approach. When the train was modeled using a dynamic moving load, the stress influence extended to approximately 5.0 m below the rail level. This relatively shallow influence depth is consistent with the rapid load application and transient nature of dynamic loading, which tends to concentrate stress within the near-surface layers due to wave attenuation and energy dissipation. In contrast, when the train load was represented using an equivalent static load, calculated via the AREEMA method, the effective depth increased to about 10.0 m. This deeper stress penetration reflects the longer load application duration and the absence of high-frequency components, allowing stress to be distributed more gradually and penetrate further into the subsoil. The difference highlights how the loading method can significantly alter the predicted stress field and, consequently, the estimated settlement behavior.

IV. CONCLUSIONS

The comparative analysis demonstrates that the HSS model provides a more realistic representation of subsoil behavior under high-speed train loading, particularly in zones of high strain near the load application. By incorporating strain-dependent stiffness and modulus degradation, the HSS model captures both the increased deformation beneath the load and the reduced settlement at low-strain regions farther from the track. In contrast, the LE model's constant stiffness assumption limits its ability to reflect true soil response, leading to underestimation in high-strain areas and overestimation in low-strain areas.

The stresses due to dynamic loading extended to a depth of 5.0 m, whereas equivalent static loading doubled this influence depth to 10.0 m, illustrating the substantial effect of loading method on stress distribution.

V.REFERENCES

[1] UIC, High Speed Rail, UIC Passenger Department, 2018.

[2] RTRI, "A study on reasonable design methods for reinforcing railroad roadbed," Special Report No. 6 (in Japanese), Japan Railway Technical Research Institute., 1996.

[3] AREMA, Chapter 1: Roadway and Ballast, Manual for Railway Engineering, USA., American Railway Engineering and Maintenance-of-Way Association, 2010.

[4] H. Lamb, "On the propagation of tremors over the surface of an elastic solid," *Philosophical Transactions Mathematical Physical & Engineering Sciences ,* vol. 203, no. 359-371, pp. 1-42, 1904.

[5] N. M. F. Araújo, High-speed trains on ballasted railway track: dynamic stress field analysis, 2011.

[6] L. Hall, Simulations and Analyses of Train-induced Ground Vibrations, 2000.

[7] J. Lysmer and R. L. Kuhlemeyer, "Finite Dynamic Model for Infinite Media," *Journal of the engineering mechanics division,* vol. 95, no. 4, pp. 859-877, 1969.

[8] W. White, I. K. Lee and V. S., "Unified boundary for finite dynamic models.," *Journal of the Engineering Mechanics Division,* vol. 103, no. 5, pp. 949-964, 1977.

[9] J. P. Wolf and C. Song, "Finite-element modelling of unbounded media," in *Proceedings of the Eleventh World Conference on Earthquake Engineering*, 1996.

[10] A. G. Correia, J. Cunha, J. Marcelino, L. Caldeira, J. Varandas, Z. Dimitrovová, A. Antão and M. Silva, "Dynamic analysis of rail track for high speed trains. 2D approach.," in *Proceedings of the 5th International Workshop on Applications of Computational Mechanics in Geotechnical Engineering*, 2007.

[11] L. Hall, "Simulations and analyses of train-induced ground vibrations in finite element models," *Soil Dynamics and Earthquake Engineering,* vol. 23, no. 5, pp. 403-413, 2003.

[12] D. Connolly, "Ground borne vibrations from high speed trains," 2013.

[13] M. Shahraki, Numerical Analysis of Soil Behavior and Stone Columns Effects on the Railway Track, Doctoral Dissertation, Bauhaus-Universität Weimar., 2019.

[14] S. Sica, F. S. de Magistris and A. Melazzo, "Free field vibrations due to the passage of high-speed trains.," in *Proceedings of the sixth european conference on numerical methods in geotechnical engineering*, Graz, Australia, 2006.

[15] G. Degrande and L. Schillemans, "Free field vibrations during the passage of a Thalys high-speed train at variable speed.," *Journal of Sound and Vibration,* vol. 247, no. 1, pp. 131-144, 2001.

[16] G. Degrande and L. Schillemans, "Free field vibrations during the passage of a Thalys high-speed train at variable speed.," *Journal of Sound and Vibration,* vol. 247, no. 1, pp. 131-144, 2001.

[17] G. Kouroussis, O. Verlinden and C. Conti, "Free field vibrations caused by high-speed: Measurement and time domain simulation," *Soil Dynamics and Earthquake Engineering,* vol. 31, no. 4, pp. 692-707, 2011.

[18] I. Chowdhury and S. P. Dasgupta, "Computation of Rayleigh damping coefficients for large systems.," *The Electronic Journal of Geotechnical Engineering,* vol. 8, no. 0, pp. 1-11, 2003.

[19] Y. M. Hashash and D. Park, "Viscous damping formulation and high frequency motion propagation in non-linear site response analysis.," *Soil Dynamics and Earthquake Engineering,* vol. 22, no. 7, pp. 611-624, 2002.

[20] D. Zhao, E. G. Nezami, Y. M. Hashash and J. Ghaboussi, "Three-dimensional discrete element simulation for granular materials," *Engineering Computations,* vol. 23, no. 7, pp. 749-770, 2006.

[21] G. Kouroussis, O. Verlinden and C. Conti, "Ground propagation of vibrations from railway vehicles using a finite/infinite-element model of the soil.," *Proceedings of the Institution of Mechanical Engineers, Part F: Journal of Rail and Rapid Transit,* vol. 223, no. 4, pp. 405-413, 2009.

[22] N. M. F. Araújo, High-speed trains on ballasted railway track: dynamic stress field analysis, 2011.

IJCRT